



HAL
open science

Multiple stages of plant root calcification deciphered by chemical and micromorphological analyses

Arnaud Huguet, Sylvain Bernard, Rime El Khatib, Martina I Gocke, Guido L B Wiesenberg, Sylvie Derenne

► To cite this version:

Arnaud Huguet, Sylvain Bernard, Rime El Khatib, Martina I Gocke, Guido L B Wiesenberg, et al.. Multiple stages of plant root calcification deciphered by chemical and micromorphological analyses. *Geobiology*, 2020, 10.1111/gbi.12416 . hal-03021321v2

HAL Id: hal-03021321



<https://hal.science/hal-03021321v2>

Submitted on 24 Nov 2020

HAL is a multi-disciplinary open access archive for the deposit and dissemination of scientific research documents, whether they are published or not. The documents may come from teaching and research institutions in France or abroad, or from public or private research centers.

L'archive ouverte pluridisciplinaire **HAL**, est destinée au dépôt et à la diffusion de documents scientifiques de niveau recherche, publiés ou non, émanant des établissements d'enseignement et de recherche français ou étrangers, des laboratoires publics ou privés.

Multiple stages of plant root calcification deciphered by chemical and micromorphological analyses

Arnaud Huguet¹  | Sylvain Bernard² | Rime El Khatib^{1,2} | Martina I. Gocke^{3,4} | Guido L. B. Wiesenberg⁴  | Sylvie Derenne¹

1
2
3 1 ABSTRACT

4 2
5 3 Rhizoliths, i.e. roots fossilized by secondary carbonates, have been known for ages and are
6
7 4 increasingly used for paleoenvironmental reconstructions. However, knowledge about their
8
9 5 formation mechanisms remains limited. This study reports the mineralogical and chemical
10
11 6 characterization of rhizoliths at different stages of mineralization and fossilization in the Late
12
13 7 Pleistocene loess-paleosol sequence of Nussloch (SW Germany). Scanning electron
14
15 8 microscopy coupled with elemental mapping and ^{13}C solid-state nuclear magnetic resonance
16
17 9 were used to concomitantly characterize the mineral and organic matter of the rhizoliths.
18
19 10 These joint analyses showed for the first time that large rhizoliths are not necessarily remains
20
21 11 of single large roots, but consist of numerous microrhizoliths as remains of fine roots, formed
22
23 12 mainly by calcium carbonates with only low amounts of Mg and Si. They further revealed
24
25 13 that the precipitation of secondary carbonates occurs not only around, but also within the plant
26
27 14 root and that fossilization leads to the selective preservation of recalcitrant root biopolymers –
28
29 15 lignin and suberin. The precipitation of secondary carbonates was observed to occur first
30
31 16 around fine roots, the epidermis acting as a first barrier, and then within the root, within the
32
33 17 cortex cells and even sometimes around the phloem and within the xylem. This study suggests
34
35 18 that the calcification of plant roots starts during the lifetime of the plant and continues after its
36
37 19 death. This has to be systematically investigated to understand the stratigraphic context before
38
39 20 using (micro)rhizoliths for paleoenvironmental reconstructions in terrestrial sediments.
40
41
42
43
44
45
46
47
48

49 22 **Keywords:** rhizoliths; SEM; ^{13}C NMR; loess sediments; secondary carbonates; organic
50
51 23 matter; paleoenvironment
52
53
54 24
55
56 25
57 26
58
59
60

1. Introduction

Rhizoliths have been ascribed different names, e.g. root casts; rhizocretions; tubular fossils (Klappa, 1980), and may exhibit different morphologies and sizes (up to several cm in diameter and several meters length; Zamanian et al., 2016). These organo-sedimentary structures are common in sandy and silty calcareous soils and sediments (Becze-Deák et al., 1997) and can be highly abundant in loess (Gocke et al., 2011) and desert sands (Sun et al., 2020). In addition to terrestrial settings, rhizoliths were also observed in former lacustrine environments (e.g. Sun et al., 2019a) and marine settings (Jones and Ng, 1988).

Rhizoliths have been used as proxies for paleoenvironmental reconstructions over different geological time scales based mainly on macro- and micromorphological studies (Becze-Deák et al., 1997; Barta, 2011) or stable carbon and oxygen isotope analyses (e.g. Kuleshov and Gavrillov, 2001). The large number of applications of these objects include understanding of past hydrological conditions (Li et al., 2015a) and vegetation composition (e.g. Koeniger et al., 2014) or pedogenesis (Driese and Mora, 1993).

Rhizoliths in loess–paleosol sequences are considered as important Quaternary paleoenvironmental archives (Becze-Deák et al., 1997). Several tools have been applied for paleoenvironmental reconstructions in such sequences, including stable isotopes ($\delta^{13}\text{C}$ and $\delta^{18}\text{O}$) of carbonates, pollen and bulk organic matter (OM) and specific compounds including lipid biomarkers (Pustovoytov and Terhorst, 2004; Frechen et al., 2007; Antoine et al., 2009; Zech et al., 2012). The underlying assumption of such studies is that the organic/inorganic signals present in sediments and paleosols were formed symsedimentarily and synpedogenically, respectively. Nevertheless, deep-rooting plants have the ability to penetrate sediments to a depth of several meters (Canadell et al., 1996). This was notably observed in several loess-(paleo)soil and sand-(paleo)soil sequences in Central and Southeast Europe (e.g. Gocke et al., 2014a), with high abundances of recent and fossilized roots (rhizoliths) as well

1
2
3 53 as root-derived biopores down to several meters depth below the recent soil or associated
4
5 54 paleosol. The post-sedimentary incorporation of root-derived OM can lead to a large overprint
6
7
8 55 of the initial signal in loess sediments, as shown for example for lipid biomarkers (e.g. *n*-
9
10 56 alkanes, fatty acids, GDGTs; Huguet et al., 2013; Gocke et al., 2014b). The presence of
11
12 57 carbonate rhizoliths in loess settings can therefore bias paleoenvironmental reconstructions.
13
14 58 Corresponding data have to be interpreted with caution, as only limited knowledge about their
15
16
17 59 formation mechanisms is available (e.g. Klappa, 1980; Gocke et al., 2011, 2014a, b; Li et al.,
18
19 60 2015b; Sun et al., 2019a; Brazier et al., 2020).

21 61 It is generally assumed that root fossilization is controlled or induced by complex organic-
22
23
24 62 inorganic interactions at the plant level (Klappa, 1980; Jaillard et al., 1991; Kautz et al., 2013;
25
26 63 Zamanian et al., 2016; Brazier et al., 2020), but the exact processes leading to the formation
27
28 64 of rhizoliths remain poorly constrained. Here, we report the chemical and micromorphological
29
30
31 65 characterization of roots at different stages of fossilization that have been sampled at different
32
33 66 depths (2.15 m, 3.5 m, 4 m and 8 m depth) from the extensively studied Late Pleistocene
34
35 67 loess-paleosol sequence of Nussloch (SW Germany) (e.g. Antoine et al., 2009; Gocke et al.,
36
37 68 2011; Zech et al., 2012; Huguet et al., 2013). The samples were chosen on the basis of their
38
39
40 69 representativeness of the rhizoliths encountered along the Nussloch profile.

41
42 70 Scanning electron microscopy (SEM) and solid-state ^{13}C Nuclear Magnetic Resonance
43
44 71 (NMR) techniques were used for the first time to describe and compare both the organic and
45
46 72 mineral structures of fresh and calcified roots from the same carbonatic setting. Based on the
47
48
49 73 chemical and structural information obtained from this joint organo-mineral characterization,
50
51 74 our main goal was to disentangle the different biomineralization stages of the formation of
52
53 75 carbonate rhizoliths of different sizes in terrestrial loess sediments.
54
55

56 76

58 77

59 78

79 2. Materials and methods

80 2.1 Study site and sampling

81 Recent and calcified roots were collected from a late Pleistocene loess–palaeosol sequence
82 at the open cast mine of HeidelbergCement AG, Nussloch, SW Germany (49.19°N, 8.43°E,
83 217 m above sea level), as described in detail by Gocke et al. (2010, 2011, 2014a, b). The
84 sampled profile comprises 13.1 m of loess and soil units, including the recent soil, with 3
85 main paleosols and 14 incipient paleosols (Gocke et al., 2014b). At the top of the profile, the
86 recent soil is developed as 0.6 m thick Vertic Cambisol Calcaric Siltic (Gocke et al., 2013).
87 The present vegetation, related to living roots, consists of natural broad-leaf forest and non-
88 native robinia (*Robinia pseudoacacia*) as well as smaller shrubs and herbaceous plants and
89 was described in detail by Gocke et al. (2013). It should be noted that present plant species
90 were most likely not the dominant plants over the past decades or centuries due to former
91 agricultural use. Rhizoliths at Nussloch were formed during various phases throughout the
92 Holocene, with ages between 3 and 10 kyr (Pustovoytov and Terhorst, 2004; Frechen et al.,
93 2007; Gocke et al., 2011) and were derived from roots of unknown trees or shrubs (likely
94 hazel, oak, beech and alder; Gocke et al., 2013). They occur continuously from the recent soil
95 to 8.8 m depth, with frequencies reaching up to 196 m⁻² at 2.55 m, and are also present below
96 10 m underneath a major paleosol (Lohne Soil) in lower frequencies (≤ 12 m⁻²; Gocke et al.,
97 2014a). They can be found in various shapes and sizes (diameter between a few mm to ca. 5
98 cm and length from mm to several m; Gocke et al., 2011).

99 Three types of samples were collected in Nussloch for comparison of the organo-mineral
100 structure of the roots: (i) present vegetation (including *Robinia pseudoacacia*); (ii) initially
101 calcified roots and (iii) rhizoliths. Initially calcified roots correspond to living roots with a
102 thin (< 1 mm) powdery carbonate coating on their surface. In contrast, samples termed as
103 “rhizoliths” are fully carbonated roots with scarce or no root remains visible to the naked eye.

1
2
3 104 Preparation of the Nussloch profile for calcified root collection implied removing at least 1
4
5 105 m of material from the top and the side of the profile, respectively, and was followed by
6
7 106 counting of roots, root-related biopores and rhizoliths on horizontal levels (Gocke et al.,
8
9 107 2014b). Rhizoliths were selected for sampling in several depth intervals where no or low
10
11 108 numbers of visible recent roots were observed in the surrounding loess, i.e. at 2.15 m, 3.5 m, 4
12
13 109 m and 8.8 m depth. Samples were collected and prepared as previously described (Gocke et
14
15 110 al., 2014b). Briefly, at each depth, intact loess cores were obtained using plastic rings with an
16
17 111 inner diameter of 20 cm and a height of 10 cm. Cores were air-dried, covered with alumina
18
19 112 foil and kept at a cool, dry place until further preparation. After having removed the plastic
20
21 113 ring, the uppermost 1 cm and outermost 1 cm of loess material was removed to avoid any
22
23 114 contamination. Then, the core was cut into concentric slices from the outer parts to the
24
25 115 interior, with the rhizolith at its center (Gocke et al., 2014b) using a ceramic knife. The
26
27 116 rhizolith was separated from the surrounding loess by tweezers and a brush, and was then
28
29 117 ground and homogenized (Gocke et al., 2011) or kept as intact rhizoliths for scanning electron
30
31 118 microscopy.
32
33
34
35
36

37 119 Last, a loess interval at 10.4 m depth was selected for sampling the so-called “initially
38
39 120 calcified roots”. The source vegetation of these fine roots is unknown, even though several
40
41 121 shrub species (mainly *Buddleja sp.*) were growing at the profile wall at ca. 8-10 m depth
42
43 122 below the recent soil. Initially calcified roots may also be present in upper layers of the
44
45 123 Nussloch sequence, but could not be discovered during profile preparation. Therefore, the
46
47 124 10.4 m horizon should only be considered as a typical depth interval, where roots at an initial
48
49 125 stage of calcification were collected. The initially calcified roots were air-dried and then
50
51 126 divided into two pieces, one of which was ground and homogenized, while the other was kept
52
53 127 as intact sample.
54
55
56
57

58 128
59
60

129 2.2 *Electron microscopy*

130 Root and rhizolith samples were impregnated with epoxy resin, cross-sectioned
131 perpendicular to their longitudinal direction, polished and gold-coated for scanning electron
132 microscopy (SEM) investigations using a Zeiss Sigma microscope operating at the
133 Laboratoire de Geologie (ENS-Paris). Backscattered electron imaging (BEI) was carried out
134 at 10kV and a working distance of 9.4 mm using an AsB detector. Energy Dispersive X-ray
135 Spectrometry (EDXS) micro-analyses were performed using INCA SmartMap™ software.
136 Elements typically encountered in secondary carbonates and surrounding loess (Ca, O, Al,
137 Mg, Si) were traced in this study.

139 2.3 *Solid state ¹³C NMR*

140 Roots from present vegetation and those with a thin carbonate crust were analyzed by ¹³C
141 NMR without any pre-treatment. In contrast, rhizoliths were treated with 3M HCl to remove
142 carbonates which would interfere with the organic carbon signal during analysis, rinsed with
143 ultrapure water and then frozen at -20 °C before being freeze-dried (Huguet et al., 2013).
144 Samples were crushed in a ball mill before analysis.

145 Solid state ¹³C cross polarization magic angle spinning nuclear magnetic resonance (CP
146 MA NMR) was performed on a Bruker Avance 500 at 125 MHz for ¹³C using 4 mm diameter
147 zircon rotors. Cross polarization allows the magnetization transfer from ¹H to ¹³C, leading to
148 an increase in the signal/noise ratio. Magic angle spinning at 14 kHz was used to reduce
149 chemical shift anisotropy and to average dipolar interactions, hence decreasing the linewidths.
150 The contact time between ¹³C and ¹H in the CP MAS sequence was set to 1 ms and the
151 repetition time to 1 s. The NMR spectra were decomposed and integrated using Dmfit
152 software – version 20150521 (Massiot et al., 2002). The subpeaks resulting from the
153 decomposition were further grouped within 6 main regions based on existing literature (e.g.

1
2
3 154 Kögel-Knabner, 2002; Lemma et al., 2007; Mathers et al., 2007): alkyl C = 0-45 ppm
4
5 155 (includes aliphatic and α -amino C); O/N-alkyl C = 45-90 ppm (includes methoxyl C and C in
6
7 156 amino groups); 90-110 ppm = di-O-alkyl C (includes anomeric C in carbohydrates); 110-140
8
9 157 ppm = aromatic and unsaturated C; 140-160 ppm = phenolic C; 160-220 ppm = carbonyl C
10
11 158 (includes carboxylic C, amides, ketones/aldehydes). More details regarding ^{13}C NMR and its
12
13 159 application to soil organic matter characterization can be found elsewhere (e.g. Knicker and
14
15 160 Nanny, 1997; Kögel-Knabner, 2002; Chukov et al., 2018).
16
17
18
19
20

21 162 **3. Results and discussion**

22 163 **3.1. Microscopic characterization of rhizoliths**

23
24 164 Rhizoliths of largely variable sizes (a few cm to m long) and diameters (a few mm to cm)
25
26 165 were observed within the Nussloch loess-paleosol sequence, as shown for example at a depth
27
28 166 of 3.5 m (Fig. 1a). It was previously reported that rhizoliths with diameters ≥ 10 mm were
29
30 167 predominant between 2 m and 6 m depth and rhizoliths with diameters < 10 mm were mainly
31
32 168 observed below 6 m (Gocke et al., 2014a). Within some of the rhizoliths, the central part of
33
34 169 the rhizolith is hollow (Fig. 1b), indicating the absence of carbonates filling the void. Even
35
36 170 though some authors tried to classify root-related structures (Klappa, 1980) or more generally
37
38 171 secondary carbonate accumulations (Barta, 2011) in terrestrial settings based on their external
39
40 172 shapes, it remains difficult to classify the diversity of calcified root structures encountered in
41
42 173 Nussloch. The general term “rhizolith” will be used here in a broad sense to refer to root
43
44 174 traces, i.e., organo-mineral structures formed through fossilization of former roots.
45
46
47
48
49

50
51 175 Typical rhizoliths from Nussloch with diameters of 10-20 mm were analyzed for their
52
53 176 internal structure. Independent of the depth, Scanning Electron Microscopy (SEM) revealed
54
55 177 the presence of numerous small, fine roots encrusted by secondary carbonates within each
56
57 178 rhizolith (e.g. Fig. 1c, f; Supp. Fig. 1). Gocke et al. (2014a) previously performed X-ray
58
59
60

1
2
3 179 microtomography scanning of one rhizolith collected at 3.5 m depth in Nussloch and observed
4
5 180 that the corresponding rhizolith contained three distinct, partially connected pores. These
6
7 181 small carbonate accumulations (diameter of <1mm) were referred to as microrhizoliths based
8
9 182 on morphological comparison with larger rhizoliths (diameter mostly 3-20 mm, up to 100
10
11 183 mm; Gocke et al., 2014a). The present SEM results further show for the first time that,
12
13 184 independent of the depth, each rhizolith that was previously assumed to be one large
14
15 185 individual calcified root, rather consists of an assemblage of numerous “microrhizoliths”,
16
17 186 which are only visible at the microscopic scale.
18
19
20

21 187 Most of these microrhizoliths roughly displayed a round shape and a central void (Fig. 1f,
22
23 188 g), indicative of the growth of the fine roots mainly in vertical direction, consistently with
24
25 189 previous observations (Gocke et al., 2011). A zoom on individual microrhizoliths reveals a
26
27 190 mosaic structure consisting of partially irregularly spread, almost concentrically arranged
28
29 191 pores and cells (Fig. 2b, c), which shows large similarities to the internal structure of recent
30
31 192 roots (Kutschera and Lichtenegger, 2002). Based on EDXS analysis, the mineral components
32
33 193 of the rhizoliths are mainly Ca-rich and Mg-poor carbonates (Fig. 3a).
34
35
36

37 194 In order to better constrain the different biomineralization processes leading to the
38
39 195 formation of the rhizoliths, the micro-elemental and -structural characteristics of
40
41 196 microrhizoliths were compared with those of (i) fresh fine roots from present vegetation at the
42
43 197 site (*Robina pseudoacacia* tree) and (ii) roots with a thin carbonate crust. These three types of
44
45 198 samples represent, in a simplified way, the different stages of the calcification process (Fig.
46
47 199 2).
48
49
50

51 200 Fresh, non-encrusted roots (Fig. 2h, i) show concentric layers of cells, with (i) a central
52
53 201 part (medulla) consisting of vascular tissues and (ii) an outer layer of cortical cells, which
54
55 202 represents the common buildup of living roots (Urry et al., 2016). The central part (Fig. 2i) is
56
57 203 characterized by secondary tissues with thick cell walls. Most of the structural characteristics
58
59
60

1
2
3 204 of the fresh tree root are still present in the initially calcified root (Fig. 2e, f). Nevertheless,
4
5 205 some differences are observed between these two types of roots. The root with a thin
6
7 206 carbonate crust (Fig. 2d-f) is characterized by (i) a thinner layer of cortical cells and (ii) larger
8
9
10 207 diameter central cells in comparison with the fresh fine root. Such differences could reflect
11
12 208 the younger age of the initially carbonated root compared to the fresh one or might be species-
13
14 209 specific. Root growth and development was indeed observed to result in the formation of
15
16 210 thicker cell walls in the central part, improving the mechanical strength, flexibility and storage
17
18 211 capacity of the roots (Raven et al., 2000; Kraus and Bascunsuelo, 2009). It can also not be
19
20 212 excluded that a part of the structural variations between the fresh and initially calcified roots
21
22 213 are due to their different origins (tree vs. unknown shrubs, respectively), as every plant
23
24 214 species can display slightly distinctive root morphological features (e.g. Basconsuelo et al.,
25
26 215 2011).

26
27
28
29
30 216 Initially calcified roots can also be distinguished from the fresh roots by the presence of
31
32 217 calcium carbonate in some of the cortex cells (Fig. 2e, f), showing that the calcification
33
34 218 process seems to initially occur within the cortical cells and not only as a coating at the
35
36 219 surface of the root. A preliminary stage is very likely the precipitation of calcium carbonate at
37
38 220 the surface of the roots, as a thin surficial carbonatic crust was observed after sampling of the
39
40 221 initially calcified roots in Nussloch (Fig. 2d), in agreement with previous observations
41
42 222 (Huguet et al., 2013). An immediate effervescence was noted when a few drops of 3M HCl
43
44 223 were added at the surface of the crust, confirming the carbonatic nature of the latter. By
45
46 224 combining these bulk and microscopic observations, we may assume that the calcification
47
48 225 process of the small roots is initiated outside the epidermis and thereafter or simultaneously
49
50 226 within the cortex cells.

51
52
53
54
55 227 A part of the initial cell and pore structure observed in the fresh root (Fig. 2h, i) was also
56
57 228 observed in microrhizoliths (Fig. 1d, e, g and Fig. 2c). Especially cortex cells filled by
58
59
60

1
2
3 229 carbonates are still visible in these microstructures (Figs. 1g and 2b), which is in agreement
4
5 230 with previous observations (Klappa, 1980; Jaillard et al., 1991; Owen et al., 2008; Cramer and
6
7 231 Hawkins, 2009). Nevertheless, in Nussloch, some of the microrhizoliths were entirely filled
8
9 232 by carbonates (e.g. the one highlighted in red in Fig. 1c). Most likely, the root cell structure is
10
11 233 preserved both in the cortical and central parts of the root (Fig. 1d, e) through the precipitation
12
13 234 of calcium carbonate (Fig. 3a). Within one single large rhizolith, numerous microrhizoliths
14
15 235 with different structures and preservation stages can be encountered. It may not be excluded
16
17 236 that all of the microrhizoliths detected at a given depth were not formed concomitantly. As we
18
19 237 did not observe any root-like concentric structures in the large rhizoliths (Fig. 1c), we can
20
21 238 exclude that a large root was responsible for the formation of the rhizolith. Either there were a
22
23 239 lot of fine roots growing inside the decaying large root after its death or numerous fine roots
24
25 240 made use of the biopore that was surviving after the decay of a former root. In both cases, the
26
27 241 largely abundant fine roots may be subsequently exposed to Ca-rich solutions in the loess,
28
29 242 leading to the carbonate encrustation and fossilization of the former fine roots. In any case,
30
31 243 there must be a decoupling of loess sedimentation and formation of large rhizoliths as the
32
33 244 latter may have occurred at any point after the formation of the large biopore that was later
34
35 245 filled by microrhizoliths, which explains the different ^{14}C ages of rhizoliths observed by
36
37 246 Gocke et al. (2011) at Nussloch.
38
39
40
41
42
43
44
45
46
47
48
49
50

51 250 **3.2. Characterization of organic matter by ^{13}C NMR**

52
53 251 Fresh fine roots, initially calcified roots and rhizoliths collected at the Nussloch loess-
54
55 252 paleosol profile were analyzed by ^{13}C NMR to investigate the effect of calcification on the
56
57 253 composition of root organic matter. The ^{13}C NMR spectrum of *R. pseudoacacia* fine roots
58
59
60

1
2
3 254 (Fig. 4a) presented in this study is similar to those spectra that were previously reported for
4
5 255 roots of various higher plants (Helfrich et al., 2006; Lemma et al., 2007; Mathers et al., 2007).
6
7 256 It was dominated by a signal ranging between 45 and 110 ppm due to N/O-alkyl C. This
8
9
10 257 region comprised two main peaks (i) at 73 ppm, which can be derived from cellulose and
11
12 258 suberin, and (ii) at 105 ppm indicative for anomeric C that can be related to hemicelluloses
13
14 259 and other carbohydrates (Baldock et al., 1992; Helfrich et al., 2006), with associated
15
16
17 260 shoulders or less intense peaks at 65, 84 and 89 ppm. This is consistent with the fact that
18
19 261 macromolecules such as cellulose, non-cellulosic carbohydrates (hemicelluloses, polyoses,
20
21 262 pectines), cutin and suberin are major components of plant tissues, especially in primary cell
22
23
24 263 walls (Albersheim, 1976). The dominant peak in the aliphatic region (0-45 ppm) was
25
26 264 observed at 30 ppm, corresponding to methylene groups present in lipids (Preston and
27
28 265 Ripmeester, 1982; Baldock et al., 1992) and macromolecules such as suberin (Gil et al.,
29
30 266 1997). Minor peaks between 25 and 35 ppm are similarly attributed to aliphatic compounds
31
32
33 267 (Helfrich et al., 2006). Broad and less intense peaks were also visible at 120-130 and 150 ppm
34
35 268 in the aromatic and O-aryl regions, respectively, and are related to aromatic molecules such as
36
37 269 lignin and tannins. The contribution of the latter type of biopolymers is further supported by
38
39
40 270 the peak at 56 ppm, which can be related to methoxyl groups (Zech et al., 1989; Parfitt and
41
42 271 Newmann, 2000). The carbonyl C region was dominated by a broad peak at 174 ppm that is
43
44 272 classically attributed to esters, carboxylic acids and amides, which can be found in lignin,
45
46
47 273 hemicelluloses, lipids and proteins (Wilson, 1987).

48
49 274 Only slight differences were observed between the ^{13}C NMR spectra of fresh and initially
50
51 275 calcified roots (Fig. 4a and b, respectively) in the 50-200 ppm region. In contrast to the fresh
52
53 276 roots (Fig. 4a), a decrease in the peak at 30 ppm and associated shoulders between 25 and 35
54
55
56 277 ppm and a slight increase in the peak at 15 ppm was noticed for the initially calcified roots
57
58 278 (Fig. 4b). ^{13}C NMR spectra of three rhizoliths (2.15 m, 3.5 m and 4 m depth) collected at
59
60

1
2
3 279 Nussloch were also recorded. However, the ^{13}C NMR signals of the rhizoliths collected at
4
5 280 2.15 m and 3.5 m depth (e.g. Supp. Fig. 2) were not sufficiently resolved and the signal to
6
7 281 noise ratio was too low for a proper interpretation. Therefore, only the ^{13}C NMR spectrum of
8
9 282 the rhizolith collected at 4 m depth will be considered in the rest of this study. It exhibited
10
11 283 broader signals in the aliphatic, O/N-alkyl and carboxylic C regions (Fig. 4c) than those from
12
13 284 fresh and initially calcified roots (Fig. 4a, b).
14
15

16
17 285 In order to refine the comparison of the ^{13}C NMR spectra, the latter were deconvoluted and
18
19 286 then integrated, thus providing an estimation of the relative abundances of the different types
20
21 287 of C functional groups (expressed in % of the total area). Obvious changes in terms of relative
22
23 288 abundances of the different C functional groups were observed between the rhizolith on the
24
25 289 one hand and other roots on the other hand (Fig. 5). The rhizolith was characterized by a
26
27 290 strong decrease in the relative abundance of the O/N-alkyl and anomeric C, along with a
28
29 291 strong increase in the relative abundance of the alkyl C and aromatic C in comparison with
30
31 292 the fresh and initially calcified roots. Such differences were reflected in the much higher
32
33 293 values of the alkyl-C/(O-alkyl + anomeric C) ratio for the rhizolith (0.60) than observed for
34
35 294 the fresh and initially calcified roots (0.27 and 0.21, respectively). This ratio is classically
36
37 295 used as a proxy for soil OM degradation (Baldock et al., 1997), based on the fact that
38
39 296 carbohydrates (i.e. O-alkyl and anomeric C) are generally the first being affected by
40
41 297 decomposition, with a concomitant increase in the relative abundance of alkyl-C related
42
43 298 possibly due to the accumulation of molecules known as recalcitrant such as suberin and its
44
45 299 derivatives (Mathers et al., 2007; White, 2018). Therefore, ^{13}C NMR spectra of the different
46
47 300 type of roots reveal that preferential degradation of cellulose and non-cellulosic
48
49 301 polysaccharides as well as enrichment in suberin occurred during or after root calcification.
50
51 302 The latter option is consistent with the partial preservation of the cell wall structure of former
52
53 303 roots through calcification, as observed by SEM (Fig. 1d, e and Fig. 2f).
54
55
56
57
58
59
60

1
2
3 304 The carboxyl C relative abundance strongly depends on the root or litter type during the
4
5 305 decomposition of OM, with an absence of trends reported for some samples (e.g. Wang et al.,
6
7 306 2013) or an increase in the carboxyl C abundance for some others (e.g. Lemma et al., 2007).
8
9 307 Such an increase was partly attributed to the oxidative cleavage of lignin (Quideau et al.,
10
11 308 2005) and/or to the accumulation of microbial fatty acids (Zech et al., 1997) during OM
12
13 309 decomposition. In Nussloch, no obvious difference in the carboxyl C abundance was observed
14
15 310 between rhizoliths, fresh and initially calcified roots (Fig. 5). This might suggest that lignin
16
17 311 was not subjected to major degradation during root calcification. This is consistent with the
18
19 312 limited fungal activity observed along most of the Nussloch sedimentary profile according to
20
21 313 phospholipid fatty acids biomarker analyses (Gocke et al., 2017), as fungi are considered to
22
23 314 play a major role in lignin degradation (Su et al., 2018). Alternatively and/or
24
25 315 complementarily, lignin might be preferentially preserved during calcification due to the
26
27 316 degradation of more easily degradable substance classes such as sugars or fatty acids
28
29 317 (Marschner et al., 2018). This is supported by the relative increase in aromatic C for rhizoliths
30
31 318 vs. fresh and initially calcified roots (Fig. 5), which may be explained by the higher intrinsic
32
33 319 chemical recalcitrance of this biopolymer vs. other compounds such as carbohydrates (Rasse
34
35 320 et al., 2005).

36
37 321 Nevertheless, one should keep in mind that preservation of specific OM components in
38
39 322 soils or sediments is dependent not only on their chemical nature but also on physical and
40
41 323 environmental parameters (e.g. Derenne and Knicker, 2000). Consequently, in the case of the
42
43 324 rhizoliths, the nature of the mineral matrix and the environmental conditions reflect the time
44
45 325 of their formation, which is consistent with the study of Brazier et al. (2020), who observed a
46
47 326 close relationship of Ca and Sr isotopes of rhizoliths with the recent soil at Nussloch.

48
49 327 In conclusion, ^{13}C NMR showed that OM is partially preserved during the formation of
50
51 328 calcified roots in Nussloch, with a selective enrichment in recalcitrant and abundant root
52
53
54
55
56
57
58
59
60

1
2
3 329 biopolymers such as lignin and suberin. This can be related to the good preservation of the
4
5 330 cell wall structure observed by electron microscopy (Figs. 1-3). Altogether, ^{13}C NMR and
6
7 331 SEM analyses suggest that the fossilization of the root by calcium carbonates was initiated
8
9 332 during the same time interval as the formation of root organic tissues (during the lifetime of
10
11 333 the root) and pursued shortly thereafter, preventing the loss of the root cell structure and
12
13 334 major degradation of OM. This is consistent with ^{14}C dating of one rhizolith from Nussloch
14
15 335 collected at 1.5 m depth, which revealed that both carbonatic and organic C ages were in the
16
17 336 same order of magnitude (3788 ± 59 years BP and 3150 ± 59 years BP, respectively), thus
18
19 337 arguing for the absence of postsegregational alteration (Gocke et al., 2011).
20
21
22
23
24
25

339 **3.3. Origin and formation of (micro)rhizoliths**

340 *3.3.1. Vegetation sources*

341 Grasses and herbaceous plants can be assumed to be potential sources of microrhizoliths
342 in the loess sequence of Nussloch (Gocke et al., 2014a), as some of these plants develop deep
343 roots (up to 2.6 m; Canadell et al., 1996), have more fine roots than trees (Jackson et al.,
344 1997) and can represent the dominant vegetation at some time periods. Nevertheless, when
345 both rhizoliths and microrhizoliths are abundant in sediments (e.g. between 1 and 6 m depth
346 in Nussloch; Gocke et al., 2014a), it is difficult to constrain the main vegetation source of
347 these calcified structures. In this case, microrhizoliths may originate not only from herbaceous
348 plants but also from fine roots of trees and shrubs based on lipid analyses (Gocke et al.,
349 2010a, 2014b) as these can have much deeper root systems up to several meters depth
350 (Canadell et al., 1996). The large, nearly round shaped structure of all rhizoliths (e.g. Fig. 1b)
351 suggests that e.g. taproots of trees formed these structures that could be traced over several
352 meters depth within the profile. It is less likely that other organisms than plants produce such
57
58
59
60

1
2
3 353 connected structures with branches similar to those in recent root systems and previously
4
5 354 visualized by computed tomography measurements (Gocke et al., 2014b).

6
7
8 355

9
10 356 *3.3.2. Proposed formation mechanism of calcified roots*

11
12 357 A formation mechanism of microrhizoliths and large rhizoliths in terrestrial loess
13
14 358 sediments can be proposed based on the results from the present study in Nussloch combined
15
16
17 359 with those of previous investigations. Three main steps can be envisioned:

18
19 360 1) After or during the growth of fine roots, a carbonate coating can develop on their
20
21 361 surface by precipitation of calcium carbonate, as suggested by bulk (HCl treatment)
22
23 362 and microscopic analyses of initially calcified roots (Fig. 2d, e, f). The initiation of the
24
25 363 calcification is directly related to rhizosphere processes and to the associated high
26
27 364 microbial activity (Jones, 1998). Roots increase acidity in the surrounding
28
29 365 soil/sediment by releasing CO₂ and exudates, which contains especially organic acids
30
31 366 (Klappa, 1980). Primary CaCO₃ from soil/sediment is dissolved and Ca²⁺ is being
32
33 367 transferred in solution towards the root. At the root surface not all calcium, magnesium,
34
35 368 strontium and other elements might be taken up by the plants as nutrients and can be
36
37 369 precipitated as secondary carbonates at the root surface (Barta, 2011). This is supported
38
39 370 by the high CO₂ concentration in the vicinity of the root due to root and microbial
40
41 371 respiration (Hinsinger et al., 2003). In addition, Ca²⁺ and Sr²⁺ from topsoils can be
42
43 372 taken up by plant roots and translocated towards larger depths in loess-paleosol
44
45 373 sequences as described by Brazier et al. (2020). Simultaneously, or after precipitation
46
47 374 of the carbonate coating on the surface of the fine roots, surplus calcium can be
48
49 375 precipitated as calcium carbonate within the cortex cells when fine roots are still alive,
50
51 376 as observed in Nussloch (Fig. 2g). Some of the fine roots may be totally infilled by
52
53 377 calcium carbonate, with precipitation around phloem and even xylem cells, as seen for
54
55
56
57
58
59
60

1
2
3 378 some of the Nussloch microrhizoliths (Fig. 3b). This disproves the assumption of some
4
5 379 authors that rhizoliths (or similar fossils like rhizogenic calcretes) are formed
6
7 380 exclusively after death and during or after decay of the root (e.g. Joseph and
8
9 381 Thrivikramaji, 2006).

10 382 2) When the precipitation of carbonates within the root continues, this may inhibit cycling
11
12 383 of water, nutrients and organic matter within roots, which might lead to death of fine
13
14 384 roots. During the decay of fine roots, organic matter as well as CO₂ gas from organic
15
16 385 matter degradation leads to a pH decrease in the rhizosphere. Under such acidic
17
18 386 conditions, dissolution and precipitation of calcium carbonate from sediment
19
20 387 weathering would take place within or around the decaying roots, resulting in the
21
22 388 mineralization and petrification of the root (e.g. Nascimento et al., 2019). Calcification
23
24 389 of the fine roots during these two steps allows at least partial preservation of the cell
25
26 390 wall structure (Figs. 1 and 2) and of the organic tissues (Figs. 4 and 5; Gocke et al.,
27
28 391 2010; Huguet et al., 2012). As fine roots have an average longevity of approximately
29
30 392 one year (Strand et al., 2008; Ding et al., 2019) and an apparent turnover of eight years
31
32 393 (Fröberg, 2012), microrhizoliths are likely formed over a short period of time (~ 1
33
34 394 year).

35
36 395 3) Concomitantly or subsequently to the previous steps, calcium carbonate may also
37
38 396 precipitate in voids between several of the fine roots. This is supported by the presence
39
40 397 of a large number of microrhizoliths within one “large” rhizolith from Nussloch with
41
42 398 precipitated carbonate in-between individual microrhizoliths (Fig. 1c, f; Supp. Fig. 1).
43
44 399 The agglomeration of microrhizoliths may be seen as a hotspot for nutrient and water
45
46 400 acquisition as well as microbial activity (Jones, 1998), and may promote the active
47
48 401 growth of new fine roots in the cavities of former large roots or potentially in-between
49
50 402 (micro-)rhizoliths, especially if they are incompletely fossilized and thus provide voids
51
52
53
54
55
56
57
58
59
60

1
2
3 403 for new root growth, which was similarly observed, e.g., in a sandy profile of Sopron
4
5 404 (NW Hungary; Huguet et al., 2013). Especially in deeper parts of the soil, biopores
6
7 405 often serve as places for renewed root growth (White and Kirkegaard, 2010). After the
8
9
10 406 death of the plants, large biopores formed by decaying roots may remain stable for
11
12 407 millennia in fine-textured sediments such as loess (Kerényi, 2015). Also in the profile
13
14 408 of Nussloch many biopores were observed throughout the whole sequence, i.e. in depth
15
16 409 intervals with high and low abundance of recent roots and rhizoliths, respectively
17
18
19 410 (Gocke et al., 2014a). Consequently, it is likely in the Nussloch sequence that
20
21 411 agglomeration of microrhizoliths occurs in biopores that were primarily produced by
22
23 412 large tap-roots of shrubs and trees. Either during the decay of these large roots or at one
24
25 413 point thereafter while still biopores were preserved, fine roots colonized the large
26
27 414 biopore or decaying root, and subsequently formation of microrhizoliths occurred by
28
29 415 the precipitation of calcium carbonate with only traces of Mg or Si (Fig. 3), whereas
30
31 416 minerals like quartz, micas or feldspars derived from primary loess were only detected
32
33 417 close to the outer rims of large rhizoliths (Gocke et al., 2011). Of course, it is possible
34
35 418 that several generations of microrhizoliths can develop in one biopore of a diameter of
36
37 419 several cm, while some older microrhizoliths might serve as additional source of
38
39 420 nutrients on top of the surrounding sediment (Brazier et al., 2020). Thus, the carbonate
40
41 421 remains might be partially destructed as indicated by the different status of
42
43 422 microrhizoliths within one large rhizolith, with (i) almost intact microrhizoliths
44
45 423 presenting perfectly round shaped structures, (ii) partially calcified microrhizoliths and
46
47 424 (iii) residual microrhizolith structures with no clear internal structure anymore (Fig. 1).

53 425 The assemblage of numerous microrhizoliths in biopores left behind after decay of former
54
55 426 larger roots led to the formation of larger rhizoliths, might have occurred during a large time
56
57 427 span starting with the development of large roots and biopores after their decay shortly after
58
59
60

1
2
3 428 sedimentation and formation of microrhizoliths at later stages. Thus, large rhizoliths in
4
5 429 Nussloch are of Holocene age (3000-9000 yrs BP) and are much younger than surrounding
6
7 430 loess deposited mainly during the last glacial-interglacial cycle (ca. 20,000 yrs BP; Gocke et
8
9 431 al., 2011). A time lag of 2 kyrs between sediment deposition and its penetration by roots was
10
11 432 also observed in a Siberian loess-like sediment (Zech et al., 2007). Similarly, in dune sands
12
13 433 (NW China), rhizoliths were of younger age than surrounding soil (Sun et al., 2019b). Even
14
15 434 small calcified root cells can be formed much later than surrounding sediment (> 10 kyrs for a
16
17 435 section close to Nussloch; Pustovoytov and Terhorst, 2004). Nevertheless, the time lag
18
19 436 between the formation of rhizoliths and the surrounding sediment will be much larger for
20
21 437 large roots compared to fine roots (several millennia vs. decades to centuries, respectively;
22
23 438 Gocke et al., 2014a). In Nussloch, several rhizoliths and microrhizoliths of different size,
24
25 439 morphology and thus very likely strongly differing age were observed within given
26
27 440 stratigraphic units, where the calcified structures were abundant (e.g. at 3.5 m, Fig. 1a). This
28
29 441 complicates the interpretation of paleoenvironmental and paleoecological data derived from
30
31 442 (micro)rhizoliths and stresses the importance of fully understanding their formation in
32
33 443 terrestrial sediments.
34
35
36
37
38
39
40
41

42 445 **4. Conclusions**

43
44 446 The organo-mineral structure of roots at different mineralization stages, collected along the
45
46 447 Nussloch loess-palesol sequence, was documented using scanning electron microscopy and
47
48 448 ¹³C solid nuclear magnetic resonance. The application of SEM and ¹³C NMR, in combination
49
50 449 with previous results, allowed for the first time the establishment of a formation model for
51
52 450 (micro)rhizoliths and consequently the assemblage of numerous microrhizoliths resulting in
53
54 451 large rhizoliths: large rhizoliths were shown to consist of numerous microrhizoliths, formed
55
56 452 mainly by calcium carbonates with only low amounts of Mg and Si. The precipitation of
57
58
59
60

1
2
3 453 secondary carbonates was observed for initially calcified roots to occur first around the fine
4
5 454 root, the epidermis acting as a first barrier, and then within the root, within the cortex cells
6
7 455 and even sometimes around the phloem and within the xylem. Fossilization of large and fine
8
9
10 456 roots by secondary carbonates was shown to allow a good preservation of root cell structure
11
12 457 and selective enrichment of recalcitrant root biopolymers such as lignin and suberin,
13
14 458 suggesting that the formation of (micro)rhizoliths may be initiated during the lifetime of the
15
16
17 459 root and continues after its death. This has to be systematically determined before using
18
19 460 (micro)rhizoliths for paleoenvironmental or paleoecological reconstructions and interpreting
20
21 461 the corresponding data with confidence. Lipid (e.g. *n*-alkanes, GDGTs, fatty acids) and
22
23 462 compound-specific isotope analyses (including radiocarbon dating) could be used to better
24
25
26 463 constrain this context.
27
28
29 464
30
31 465
32
33 466
34
35 467
36 468
37 469
38 470
39 471
40 472
41 473
42 474
43 475
44 476
45 477
46 478
47 479
48 480
49 481
50 482
51 483
52 484
53 485
54 486
55 487
56 488
57 489

490 **References**

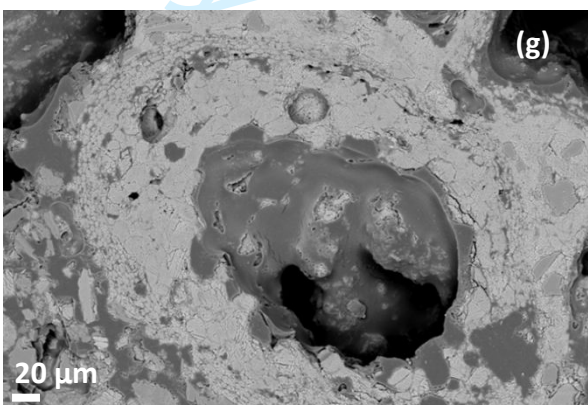
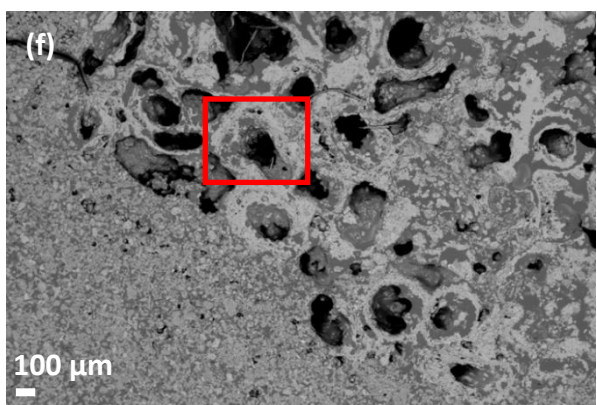
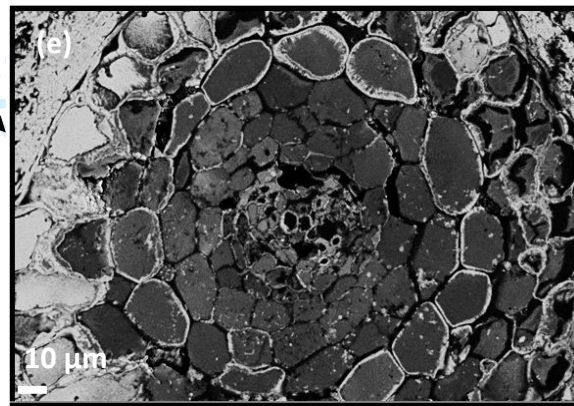
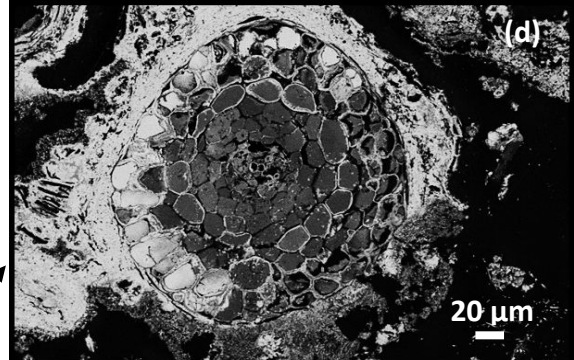
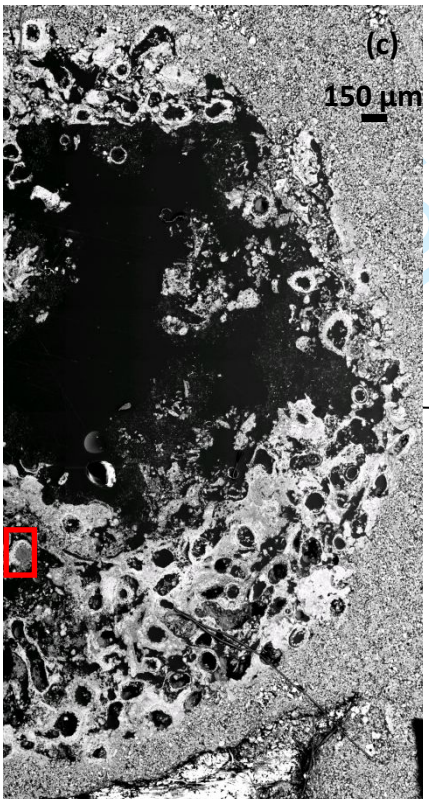
- 491
- 492 Albersheim, P. (1976). The primary cell wall. In: Plant Biochemistry, Bonner and Varner eds.
493 3rd Edition, Academic Press, New York, 225-274.
- 494 Antoine, P., Rousseau, D.D., Moine, O., Kunesch, S., Hatté, C., Lang, A., Tissoux, H., Zöller,
495 L. (2009). Rapid and cyclic aeolian deposition during the Last Glacial in European loess: a
496 high-resolution record from Nussloch, Germany. *Quaternary Science Reviews*, 28, 2955–
497 2973.
- 498 Baldock, J.M., Oades, J.M., Waters, A.G., Peng, X., Vassallo, A.M., Wilson, M.A. (1992).
499 Aspects of the chemical structure of soil organic materials as revealed by solid-state ¹³C
500 NMR spectroscopy. *Biogeochemistry*, 16, 1-42.
- 501 Baldock, J.A., Oades, J.M., Nelson, P.N., Skene, T.M., Golchin, A., Clarke, P. (1997).
502 Assessing the extent of decomposition of natural organic materials using solid state ¹³C
503 NMR spectroscopy. *Australian Journal of Soil Research*, 35, 1061–1083.
- 504 Barta, G. (2011). Secondary carbonates in loess-paleosol sequences: a general review.
505 *Central European Journal of Geosciences* 3, 129–146.
- 506 Basconsuelo, S., Grosso, M., Molina, M.G., Malpassi, R., Kraus, T., Bianco, C., 2011.
507 Comparative root anatomy of papilionoid Legumes. *Flora*, 206, 799-807.
- 508 Becze-Deák, J., Langohr, R., Verrecchia, E. (1997). Small scale secondary CaCO₃
509 accumulations in selected sections of the European loess belt: morphological forms and
510 potential for paleoenvironmental reconstruction. *Geoderma*, 76, 221-252.
- 511 Bindschedler, S., Cailleau, G., Verrecchia, E. (2016). Role of fungi in the biomineralization of
512 calcite. *Minerals*, 6, 41.
- 513 Brazier, J.-M., Schmitt, A.D., Gangloff, S., Pelt, E., Gocke, M.I., Wiesenberg, G.L.B. (2020).
514 Multi-isotope approach ($\delta^{44}/40\text{Ca}$, $\delta^{88}\text{Sr}$ and $87\text{Sr}/86\text{Sr}$) provides insights into rhizolith
515 formation mechanisms in terrestrial sediments of Nussloch (Germany). *Chemical Geology*
516 545, 119641.
- 517 Canadell, J., Jackson, R.B., Ehleringer, J.R., Mooney, H.A., Sala, O.E., Schulze, E.D. (1996).
518 Maximum rooting depth of vegetation types at the global scale. *Oecologia*, 108, 583–595.
- 519 Chukov, S.N., Lodygin, E.D., Abakumov (2018). Application of ¹³C NMR spectroscopy to
520 the study of soil organic matter: A review of publications. *Eurasian Soil Science* 51, 889-
521 900.
- 522 Cramer, M.D., Hawkins, H.J (2009). A physiological mechanism for the formation of root
523 casts. *Palaeogeography, Palaeoclimatology, Palaeoecology*, 274, 125–133.
- 524 Derenne, S., Knicker, H. (2000). Chemical structure and preservation processes of organic
525 matter in soils and sediments. *Organic Geochemistry*, 31, 607-608.
- 526 Ding, Y., Leppälammı-Kujansuu, J., Helmisaari, H.-S. (2019). Fine root longevity and below-
527 and aboveground litter production in a boreal *Betula pendula* forest. *Forest Ecology and*
528 *Management*, 431, 17-25.
- 529 Driese, S.G., Mora, C.I. (1993). Physico-chemical environment of pedogenic carbonate
530 formation in Devonian vertic palaeosols, central Appalachians, USA. *Sedimentology*, 40,
531 199–216.
- 532 Frechen, M., Terhorst, B., Rähle, W. (2007). The Upper Pleistocene loess/palaeosol sequence
533 from Schatthausen in North Baden–Württemberg. *Quaternary Science Journal*, 56, 212–227.
- 534 Fröberg, M. (2012). Residence time of fine-root carbon using radiocarbon measurements of
535 samples collected from a soil archive. *Journal of Plant Nutrition and Soil Science*, 175, 46–
536 48.
- 537 Gil, A.M., Lopes, M., Rocha, J., Pascoal Neto, C. (1997). A ¹³C solid state nuclear magnetic
538 resonance spectroscopic study of cork cell wall structure: the effect of suberin removal.
539 *International Journal of Biological Macromolecules*, 20, 293-305.

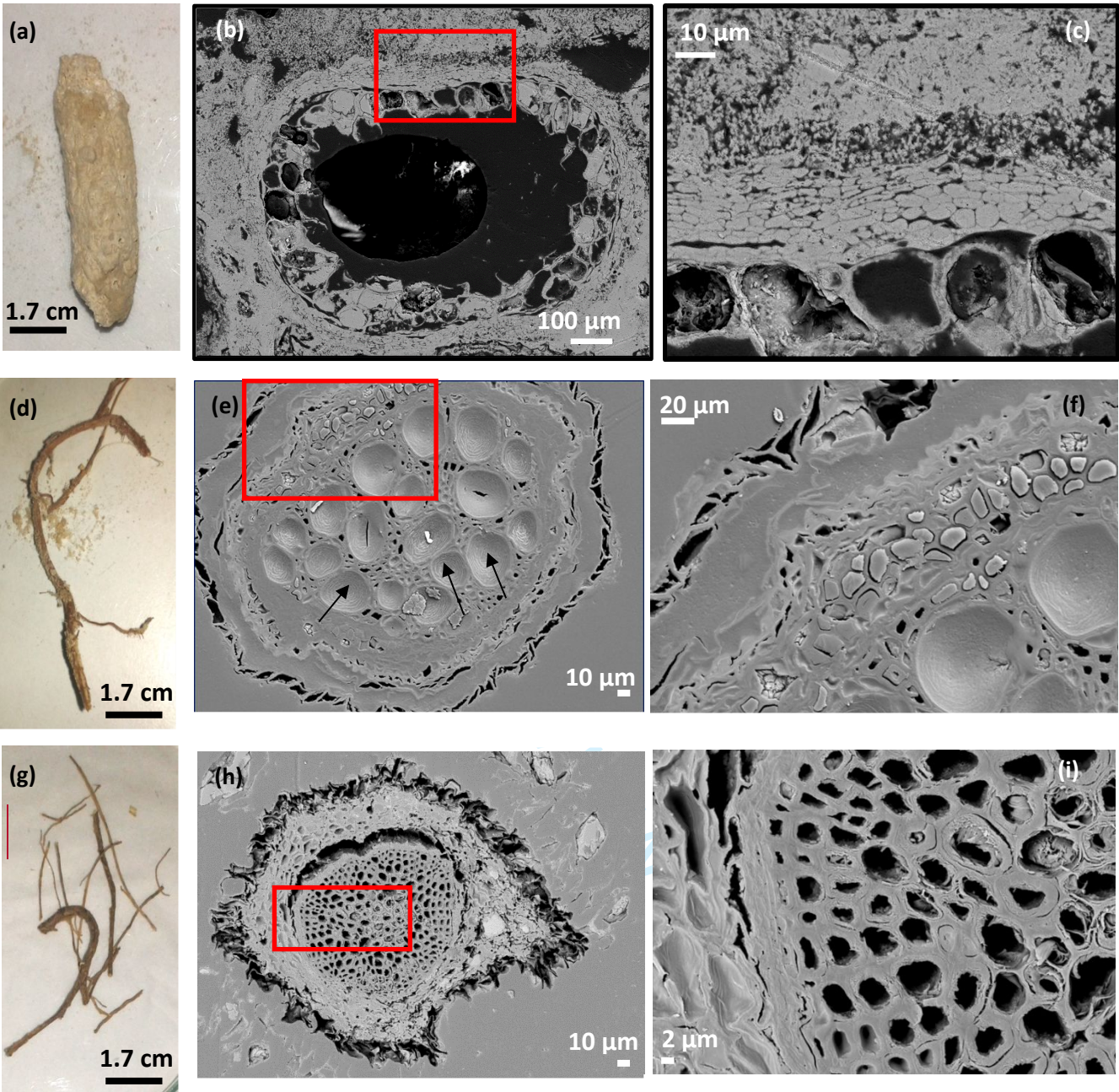
- 1
2
3 540 Gocke, M., Wiesenberg, G.L.B., Pustovoytov, K., Kuzyakov, Y. (2010). Rhizoliths in loess –
4 541 evidence for post-sedimentary incorporation of root-derived organic matter in terrestrial
5 542 sediments as assessed from molecular proxies. *Organic Geochemistry*, 41, 1198-1206.
- 6 543 Gocke, M., Pustovoytov, K., Kühn, P., Wiesenberg, G.L.B., Löscher, M., Kuzyakov, Y.
7 544 (2011). Carbonate rhizoliths in loess and their implications for paleoenvironmental
8 545 reconstruction revealed by isotopic composition: $\delta^{13}\text{C}$, ^{14}C . *Chemical Geology*, 283, 251-
9 546 260.
- 10 547 Gocke, M., Kuzyakov, Y., Wiesenberg, G.L.B. (2013). Differentiation of plant derived
11 548 organic matter in soil, loess and rhizoliths based on *n*-alkane molecular proxies.
12 549 *Biogeochemistry*, 112, 23-40.
- 13 550 Gocke, M., Gulyás, S., Hambach, U., Jovanović, M., Kovács, G., Marković, S.B.,
14 551 Wiesenberg, G.L.B. (2014a). Biopores and root features as new tools for improving
15 552 paleoecological understanding of terrestrial sediment-paleosol sequences. *Palaeogeography*,
16 553 *Palaeoclimatology*, *Palaeoecology*, 394, 42-58.
- 17 554 Gocke, M., Peth, S., Wiesenberg, G.L.B. (2014b). Lateral and depth variation of loess organic
18 555 matter overprint related to rhizoliths revealed by lipid molecular proxies and X-ray
19 556 tomography. *Catena*, 112, 72-85.
- 20 557 Gocke, M.I., Huguet, A., Derenne, S., Kolb, S., Dippold, M., Wiesenberg, G.L.B. (2017).
21 558 Disentangling interactions between microbial communities and roots in deep subsoil.
22 559 *Science of the Total Environment*, 575, 135-145.
- 23 560 Graça, J. (2015). Suberin: the biopolyester at the frontier of plants. *Frontiers in Chemistry*, 3,
24 561 62. <https://doi.org/10.3389/fchem.2015.00062>
- 25 562 Helfrich, M., Ludwig, B., Buurman, P., Flessa, H. (2006). Effect of land use on the
26 563 composition of soil organic matter in density and aggregate fractions as revealed by solid-
27 564 state ^{13}C NMR spectroscopy. *Geoderma*, 136, 331-341.
- 28 565 Hinsinger, P., Plassard, C., Tang, C., Jaillard, B. (2003). Origins of root-mediated pH changes
29 566 in the rhizosphere and their responses to environmental constraints: a review. *Plant and Soil*
30 567 248, 43–59.
- 31 568 Huguet, A., Wiesenberg, G.L.B., Gocke, M., Fosse, C., Derenne, S. (2012). Branched
32 569 tetraether membrane lipids associated with rhizoliths in loess: rhizomicrobial overprinting
33 570 of initial biomarker record. *Organic Geochemistry*, 43, 12-19.
- 34 571 Huguet, A., Gocke, M., Derenne, S., Fosse, C., Wiesenberg, G.L.B. (2013). Root-associated
35 572 branched tetraether source microorganisms may reduce estimated paleotemperatures in
36 573 subsoil. *Chemical Geology*, 356, 1–10.
- 37 574 Jackson, R.B., Mooney, H.A., Schulze, E.D. (1997). A global budget for fine root biomass,
38 575 surface area, and nutrient contents. *Proceedings of the National Academy of Sciences of the*
39 576 *United States of America*, 94, 7362–7366.
- 40 577 Jaillard, B., Guyon, A., Maurin, A.F. (1991). Structure and composition of calcified roots, and
41 578 their identification in calcareous soils. *Geoderma*, 50, 197-210.
- 42 579 Jones, D.L. (1998). Organic acids in the rhizosphere – a critical review. *Plant and Soil*, 205,
43 580 25–44.
- 44 581 Jones, B., Ng, K.-C. (1988). The structure and diagenesis of rhizoliths from Cayman Brac,
45 582 British West Indies. *Journal of Sedimentary Research* 58, 457-467.
- 46 583 Joseph, S., Thirvikramaji, K.P. (2006). Rhizolithic calcrete in Teris, southern Tamil Nadu:
47 584 origin and paleoenvironmental implications. *Journal of the Geological Society of India* 65,
48 585 158–168
- 49 586 Kerényi, A. (2015). Chapter 25. Loess Features on Tokaj Hill, in: Lóczy, D. (Ed.),
50 587 *Landscapes and Landforms of Hungary*. Springer, Heidelberg, pp. 219–226.
- 51 588 Klappa, C.F. (1980). Rhizoliths in terrestrial carbonates: classification, recognition, genesis,
52 589 and significance. *Sedimentology*, 27, 613-629.

- 1
2
3 590 Knicker, H., Nanny, M.A. (1997). Nuclear magnetic resonance spectroscopy: Basic theory
4 591 and background. In: NMR spectroscopy in environmental science and technology. Nanny,
5 592 M.A., Minear, R.A., Leenheer, J.A. (Eds). Oxford University Press, London, 3-15.
6 593 Koeniger, P., Barta, G., Thiel, C., Bajnóczi, B., Novothny, Á., Horváth, E., Techmer, A.,
7 594 Frechen, M. (2014). Stable isotope composition of bulk and secondary carbonates from the
8 595 Quaternary loess–palaeosol sequence in Sütto, Hungary. *Quaternary International*, 319, 38-
9 596 49.
10 597 Kögel-Knabner, I. (2002). The macromolecular organic composition of plant and microbial
11 598 residues as inputs to soil organic matter. *Soil Biology & Biochemistry*, 34, 139–162.
12 599 Kraus, T., Basconsuelo, S. (2009). Secondary root growth in *Rhynchosia edulis* Griseb.
13 600 (Leguminosae): origin of cambia and their products. *Flora*, 204, 635-643.
14 601 Kuleshov, V.N., Gavrillov, Y.O. (2001). Isotopic composition ($\delta^{13}\text{C}$, $\delta^{18}\text{O}$) of carbonate
15 602 concretions from terrigenous deposits in the Northern Caucasus. *Lithology and Mineral
16 603 Resources*, 36, 160–163.
17 604 Kutschera L., Lichtenegger E. (2002). *Wurzelatlas mitteleuropäischer Waldbäume und
18 605 Sträucher*. Stocker Leopold Verlag, 604 pp.
19 606 Lemma, B., Nilsson, I., Kleja, D.B., Olsson, M., Knicker, H. (2007). Decomposition and
20 607 substrate quality of leaf litters and fine roots from three exotic plantations and a native
21 608 forest in the southwestern highlands of Ethiopia. *Soil Biology and Biochemistry*, 39, 2317-
22 609 2328.
23 610 Li, Z., Wang, N., Li, R., Ning, K., Cheng, H., Zhao, L. (2015a). Indication of millennial-scale
24 611 moisture changes by the temporal distribution of Holocene calcareous root tubes in the
25 612 deserts of the Alashan Plateau, Northwest China. *Palaeogeography Palaeoclimatology
26 613 Palaeoecology*, 440, 496–505.
27 614 Li, Z., Wang, N., Cheng, H., Ning, K., Zhao, L., Li, R. (2015b). Formation and environmental
28 615 significance of late Quaternary calcareous root tubes in the deserts of the Alashan Plateau,
29 616 northwest China. *Quaternary International*, 372, 165-174.
30 617 Massiot, D., Fayon, F., Capron, M., King, I., Le Calvé, S., Alonso, B., Durand, J.-O., Bujoli,
31 618 B., Gan, Z., Hoatson, G. (2002). Modelling one- and two-dimensional solid-state NMR
32 619 spectra. *Magnetic Resonance in Chemistry*, 40, 70–76.
33 620 Marschner B, Brodowski S, Dreves A, Gleixner, G., Gude, A., Grootes, P.M., Hamer, U.,
34 621 Heim, A., Jandl, G., Ji, R., Kaiser, K., Kalbitz, K., Kramer, C., Leinweber, P., Rethemeyer,
35 622 J., Schäffer, A., Schmidt, M.W.I., Schwark, L., Wiesenberg, G.L.B. (2008). How relevant is
36 623 recalcitrance for the stabilization of organic matter in soils? *Journal of Plant Nutrition and
37 624 Soil Science* 171, 91-110.
38 625 Mathers, N.J., Jalota, R.K., Dalal, R.C., Boyd, S.E. (2007). ^{13}C -NMR analysis of
39 626 decomposing litter and fine roots in the semi-arid Mulga Lands of southern Queensland.
40 627 *Soil Biology & Biochemistry*, 39, 993–1006.
41 628 Nascimento, D.L., Batezelli, A., Ladeira, F.S. (2019). The paleoecological and
42 629 paleoenvironmental importance of root traces: Plant distribution and topographic
43 630 significance of root patterns in Upper Cretaceous paleosols. *Catena* 172, 789–806.
44 631 Owen, R.A., Owen, R.B., Renaut, R.W., Scott, J., Jones, B., Ashley, G.M. (2008).
45 632 Mineralogy and origin of rhizoliths on the margins of saline, alkaline Lake Bogoria, Kenya
46 633 Rift Valley. *Sedimentary Geology*, 203, 143–163.
47 634 Parfitt, R.L., Newman, R.H. (2000). ^{13}C NMR study of pine needle decomposition. *Plant Soil*,
48 635 219, 273–278.
49 636 Preston, C.M., Ripmeester, J.A. (1982). Application of solution and solid-state ^{13}C NMR to
50 637 four organic soils, their humic acids, fulvic acids, humins and hydrolysis residues. *Canadian
51 638 Journal of Spectroscopy*, 27, 99–105.
52
53
54
55
56
57
58
59
60

- 1
2
3 639 Pustovoytov, K., Terhorst, B. (2004). An isotopic study of a late Quaternary loess–paleosol
4 640 sequence in SW Germany. *Revista Mexicana de Ciencias Geológicas*, 21, 88–93.
- 5 641 Quideau, S.A., Graham, R.C., Oh, S.W., Hendrix, P.F., Wasylishen, R.E. (2005). Leaf litter
6 642 decomposition in a chaparral ecosystem, Southern California. *Soil Biology & Biochemistry*,
7 643 37, 1988-1998.
- 8 644 Raven, P.H., Evert, R.F., Eichhorn, S.E. (2000). *Biologie végétale*, 6th edition. De Boeck
9 645 Université editions.
- 10 646 Strand, A.E., Pritchard, S.G., McCormack, M.L., Davis, M.A., Oren, R. (2008). Irreconcilable
11 647 differences: fine root lifespans and soil carbon persistence. *Science*, 319, 456–458.
- 12 648 Su, Y., Yu, X., Sun, Y., Wang, G., Chen, H., Chen, G. (2018). Evaluation of screened lignin-
13 649 degrading fungi for the biological pretreatment of corn stover. *Scientific Reports* 8, 5385.
- 14 650 Sun, Q., Xue, W., Zamanian, K., Colin, C., Duchamp-Alphonse, S., Pei, W. (2019a).
15 651 Formation and paleoenvironment of rhizoliths of Shiyang River Basin, Tenggeri Desert, NW
16 652 China. *Quaternary International*, 502, 246-257.
- 17 653 Sun, Q., Wang, H., Zamanian, K. (2019b). Radiocarbon age discrepancies between the
18 654 carbonate cement and the root relics of rhizoliths from the Badain Jaran and the Tenggeri
19 655 deserts, Northwest China. *Catena*, 180, 263-270.
- 20 656 Sun, Q., Zamanian, K., Huguet, A., Fa, K., Wang, H. (2020). Characterization and formation
21 657 of the pristine rhizoliths around *Artemisia* roots in dune soils of Tenggeri Desert, NW China.
22 658 *Catena* 193, 104633.
- 23 659 Urry, L.A., Cain, M.L., Wasserman, S.A., Minorsky, P.V., Reece, J.B. (2016). *Campbell*
24 660 *Biology*, 11th Edition, Chap. 35: Vascular plant structure, growth and development. Pearson
25 661 Eds.
- 26 662 Wang, H., Liu, S., Wang, J., Shi, Z., Lu, L., Guo, W., Jia, H., Cai, D. (2013). Dynamics and
27 663 speciation of organic carbon during decomposition of leaf litter and fine roots in four
28 664 subtropical plantations of China. *Forest Ecology and Management*, 300, 43-52.
- 29 665 White, R.G., Kirkegaard, J.A. (2010). The distribution and abundance of wheat roots in a
30 666 dense, structured subsoil—implications for water uptake. *Plant, Cell & Environment*, 33,
31 667 133–148.
- 32 668 White, K.E., Coale, F.J., Reeves III, J.B. (2018). Degradation changes in plant root cell wall
33 669 structural molecules during extended decomposition of important agricultural crop and
34 670 forage species. *Organic Geochemistry*, 115, 233-245.
- 35 671 Wilson, M.A. (1987). *NMR Techniques and Applications in Geochemistry and Soil*
36 672 *Chemistry*. Pergamon Press, Oxford. 353 pp.
- 37 673 Zamanian, K., Pustovoytov, K., Kuzyakov, Y. (2016). Pedogenic carbonates: Forms and
38 674 formation processes. *Earth-Science Reviews*, 157, 1-17.
- 39 675 Zech, W., Haumaier, L., Kögel-Knabner, I. (1989). Changes in aromaticity and carbon
40 676 distribution of soil organic matter due to pedogenesis. *Science of the Total Environment*,
41 677 81/82, 179–186.
- 42 678 Zech, M., Rass, S., Buggle, B., Löscher, M., Zöller, L. (2012). Reconstruction of the late
43 679 Quaternary paleoenvironments of the Nussloch loess paleosol sequence, Germany, using *n*-
44 680 alkane biomarkers. *Quaternary Research*, 78, 226-235.
- 45 681 Zech, W., Senesi, N., Guggenberger, G., Kaiser, K., Lehmann, J., Miano, T.M., Miltner, A.,
46 682 Schroth, G. (1997). Factors controlling humification and mineralization of soil organic
47 683 matter in the tropics. *Geoderma*, 79, 117-161.
- 48 684 Zech, M., Zech, R., Glaser, B. (2007). A 240,000-year stable carbon and nitrogen isotope
49 685 record from a loess-like palaeosol sequence in the Tumara Valley, Northeast Siberia.
50 686 *Chemical Geology*, 242, 307–318.
- 51 687
52 688

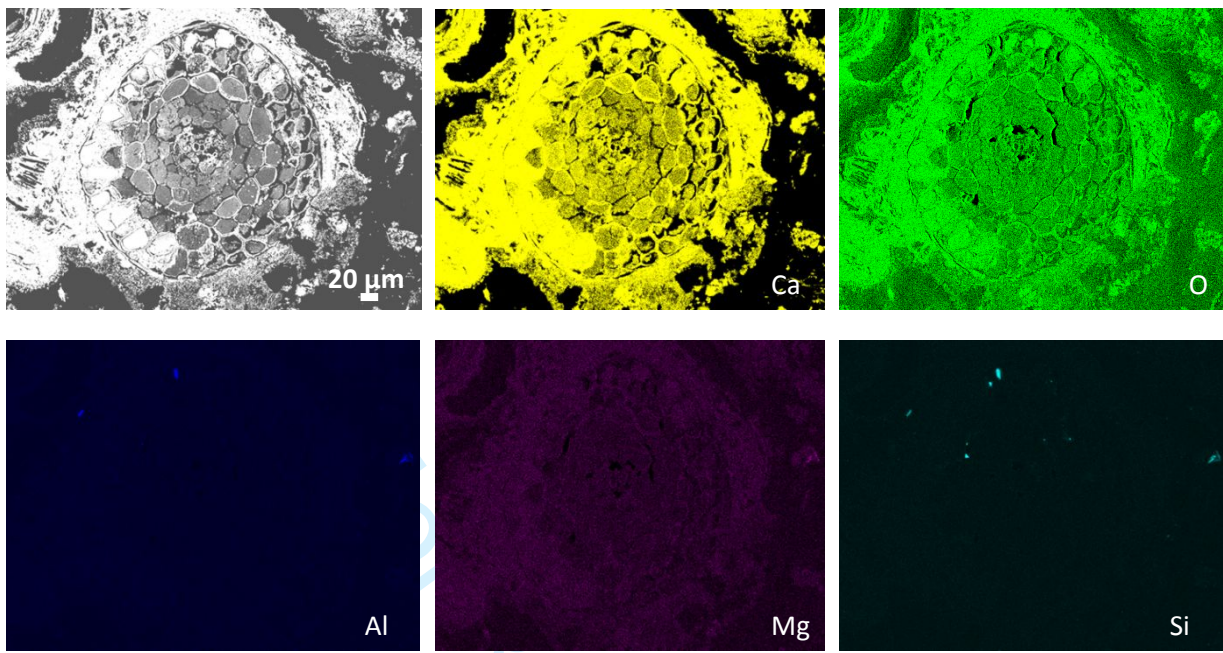
1
2
3
4
5
6
7
8
9
10
11
12
13
14
15
16
17
18
19
20
21
22
23
24
25
26
27
28
29
30
31
32
33
34
35
36
37
38
39
40
41
42
43
44
45
46
47
48
49
50
51
52
53
54
55
56
57
58
59
60



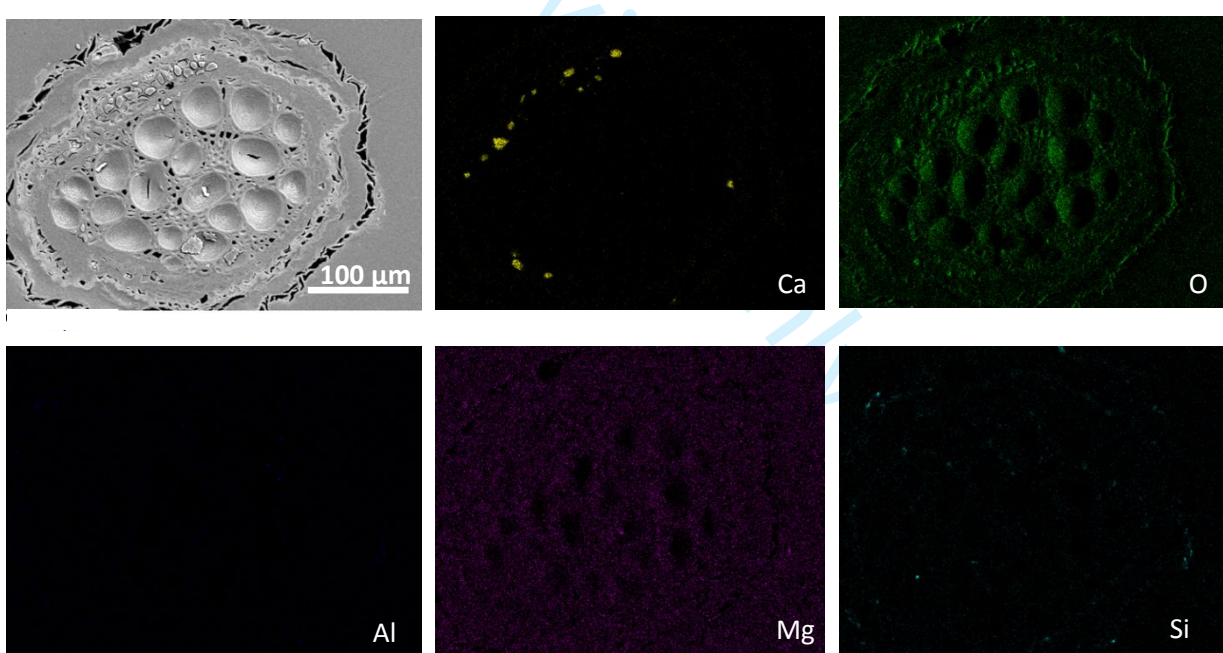


1
2
3
4
5
6
7
8
9
10
11
12
13
14
15
16
17
18
19
20
21
22
23
24
25
26
27
28
29
30
31
32
33
34
35
36
37
38
39
40
41
42
43
44
45
46
47
48
49
50
51
52
53
54
55
56
57
58
59
60

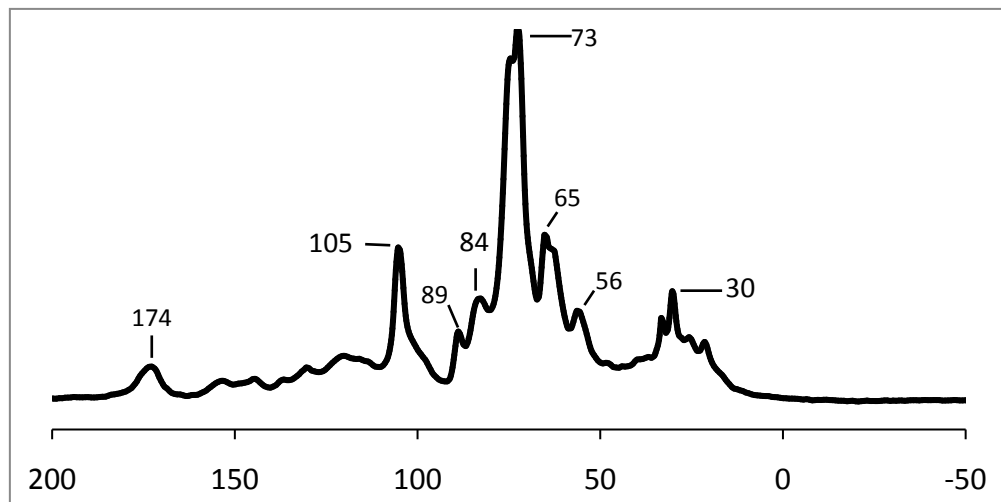
(a)



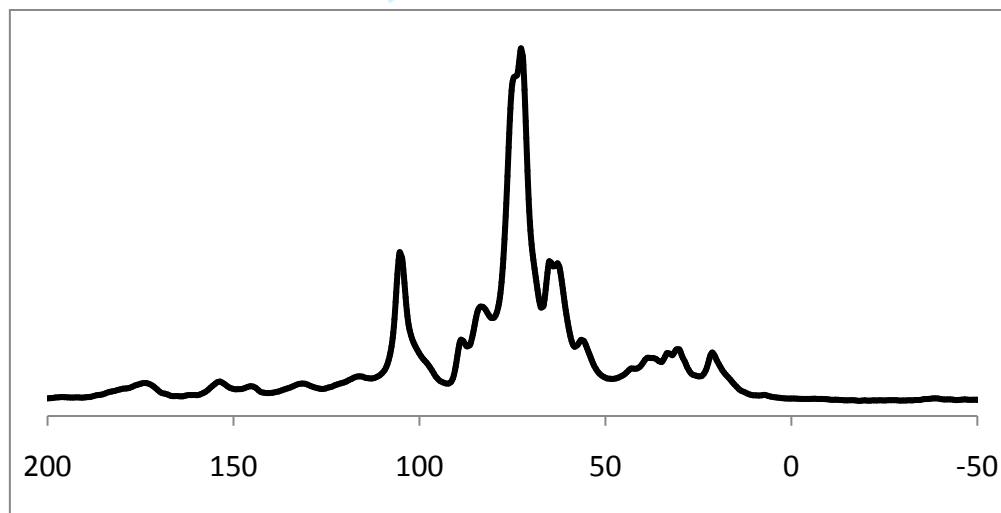
(b)



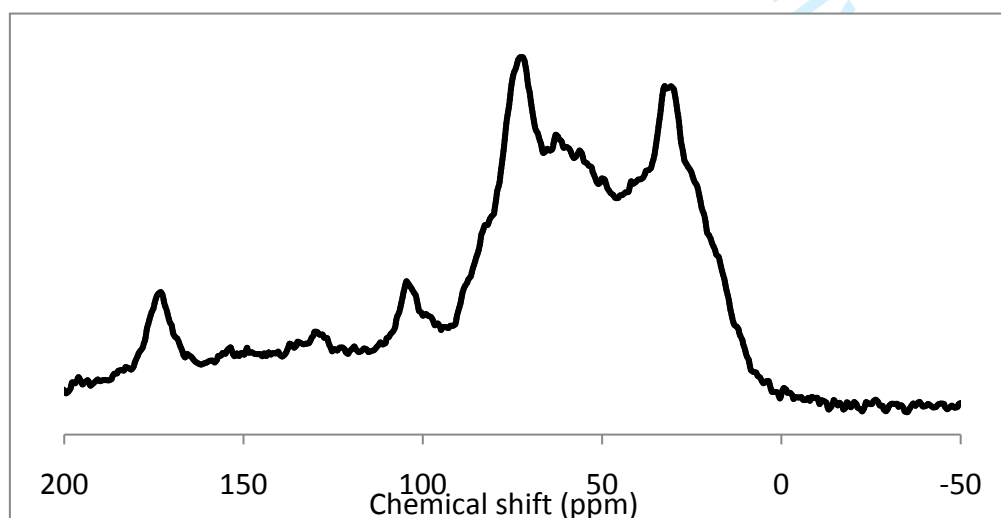
(a)



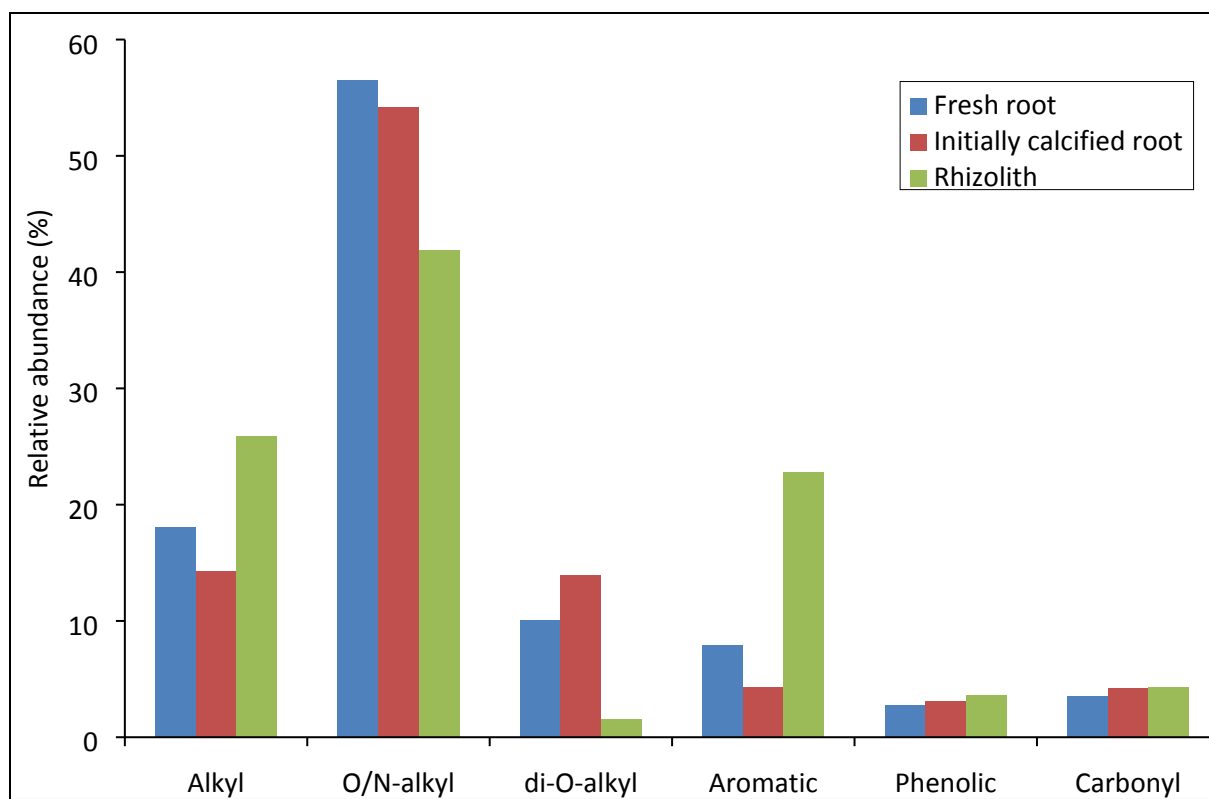
(b)



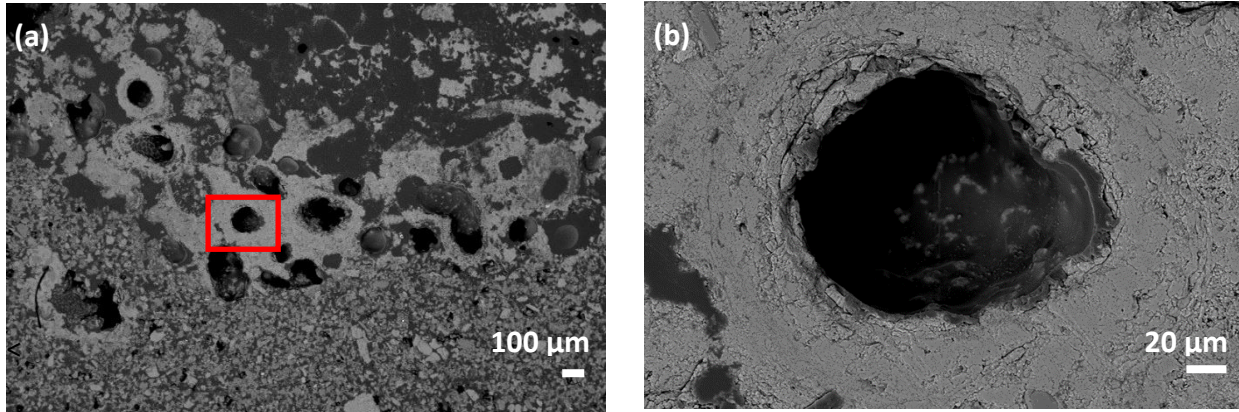
(c)



1
2
3
4
5
6
7
8
9
10
11
12
13
14
15
16
17
18
19
20
21
22
23
24
25
26
27
28
29
30
31
32
33
34
35
36
37
38
39
40
41
42
43
44
45
46
47
48
49
50
51
52
53
54
55
56
57
58
59
60

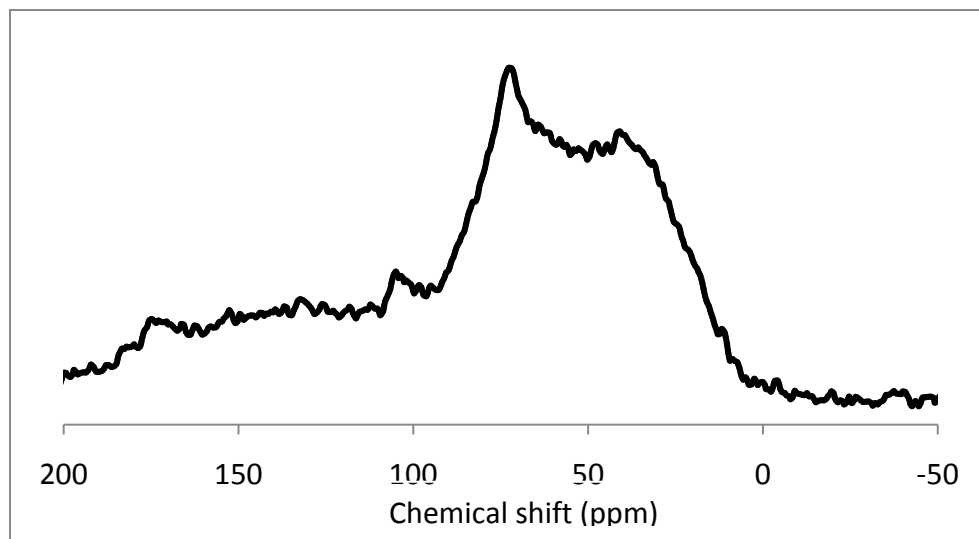


Review Only



Supp. Fig. 1. Scanning electron micrographs showing the structure of rhizolith collected at 2.15 m depth in cross section. The zone highlighted in red in panel (a) was enlarged for better visualization of the rhizolith internal structure (cf. panel (b)).

For Review Only



Supp. Fig. 2. ^{13}C NMR spectrum of rhizolith collected at 2.15 m depth in Nussloch (SW Germany).

For Review Only